Current Research in Pharmacology and Drug Discovery 4 (2023) 100147

Contents lists available at ScienceDirect

Current Research in Pharmacology and Drug Discovery

journal homepage: www.journals.elsevier.com/current-research-in-pharmacology-and-drug-discovery

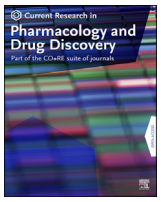

A novel drug-like water-soluble small molecule Focal Adhesion Kinase (FAK) activator promotes intestinal mucosal healing

Qinggang Wang [a,1], Ricardo Gallardo-Macias [b,1], Emilie E. Vomhof-DeKrey [a], Rashmi Gupta [c], Svetlana A. Golovko [d], Mikhail Y. Golovko [d], Sema Oncel [d], Vadim J. Gurvich [b], Marc D. Basson [e,*]

[a] Department of Surgery, University of North Dakota School of Medicine and Health Sciences, USA
[b] Institute for Therapeutics Discovery and Development and Department of Medicinal Chemistry, College of Pharmacy, University of Minnesota, USA
[c] Currently at Department of Biology, University of Maryland, USA
[d] Department of Biomedical Sciences, University of North Dakota School of Medicine and Health Sciences, USA
[e] Departments of Surgery, Biomedical Sciences, and Pathology, University of North Dakota School of Medicine and Health Sciences, USA

ARTICLE INFO

Keywords:
Non-steroidal anti-inflammatory drugs
Focal adhesion kinase
Mucosal healing
Small intestine
Ulcer

ABSTRACT

Non-steroidal anti-inflammatory drugs (NSAIDs) injure the proximal and distal gut by different mechanisms. While many drugs reduce gastrointestinal injury, no drug directly stimulates mucosal wound healing. Focal adhesion kinase (FAK), a non-receptor tyrosine kinase, induces epithelial sheet migration.

We synthesized and evaluated a water-soluble FAK-activating small molecule, M64HCl, with drug-like properties. Monolayer wound closure and Western blots measured migration and FAK phosphorylation in Caco-2 cells, in vitro kinase assays established FAK activation, and pharmacologic tests assessed drug-like properties. 30 mg/kg/day M64HCl was administered in two murine small intestine injury models for 4 days.

M64HCl (0.1–1000 nM) dose-dependently increased Caco-2 FAK-Tyr 397 phosphorylation, without activating Pyk2 and accelerated Caco-2 monolayer wound closure. M64HCl dose-responsively activates the FAK kinase domain vs. the non-salt M64, increasing the V_{max} of ATP-binding. Pharmacologic tests suggested M64HCl has drug-like properties and is enterally absorbed. M64HCl 25 mg/kg/day continuous infusion promoted healing of ischemic jejunal ulcers and indomethacin-induced small intestinal injury in C57Bl/6 mice. M64HCl-treated mice exhibited smaller ulcers 4 days after ischemic ulcer induction or indomethacin injury. Renal histology and plasma creatinine were normal. Mild hepatic inflammatory changes and ALT elevation were similar among M64HCl-treated mice and controls. M64HCl was concentrated in kidney and gastrointestinal mucosa and functional nephrectomy studies suggested predominantly urinary excretion. Little toxicity was observed in vitro or in single-dose mouse toxicity studies until >1000x higher than effective concentrations. M64HCl, a water-soluble FAK activator, promotes epithelial restitution and intestinal mucosal healing and may be useful to treat gut mucosal injury.

1. Introduction

Aspirin and other nonsteroidal anti-inflammatory drugs (NSAIDs) have long been known to injure the gastroduodenal mucosa but are now known to injure the distal small bowel injury at even higher rates. 10–40% and 50% of chronic NSAID users develop upper or lower GI ulcers respectively (Yamagata and Hiraishi, 2007, Higuchi et al., 2009; Endo et al., 2015). NSAID-associated enteropathy has gained much attention due to the introduction of new diagnostic devices such as video capsule endoscopy and device-assisted enteroscopy (Maiden, 2009; Scarpignato and Bjarnason, 2019, Lim et al., 2020). Erosive lesions are observed throughout the small intestine when low dose aspirin users are subjected to capsule endoscopy in low dose aspirin users (Iwamoto et al., 2014). NSAID-induced lower GI (LGI) injury can cause acute bleeding or chronic anemia, perforation, stricture, or obstruction (Watanabe et al., 2020). Unfortunately, the cost of video capsule endoscopy has limited its widespread use, so NSAID enteropathy continues to be underdiagnosed (Meltzer et al., 2014).

* Corresponding author. Departments of Surgery, Biomedical Sciences, and Pathology, University of North Dakota School of Medicine and Health Sciences, 1301 North Columbia Road, Stop 9037, Grand Forks, ND, 58202-9037, USA.
E-mail address: Marc.basson@und.edu (M.D. Basson).
[1] To be considered co-first authors.

https://doi.org/10.1016/j.crphar.2022.100147

Proton pump inhibitors (PPIs) have been co-prescribed with NSAIDs to ameliorate proximal GI NSAID injury (Wallace et al., 2011; Tran-Duy et al., 2015; Gwee et al., 2018). However, we now know that gastric acid suppression cannot protect or repair NSAID-induced distal intestinal damage (Zhang et al., 2013), and indeed actually worsens NSAID small bowel enteropathy (Washio et al., 2016) at least in part because of changes in the number and types of bacteria in the small intestine during proton pump inhibitor therapy (Wallace, 2012, Imhann et al., 2016). PPIs are therefore no longer recommended to prevent NSAID injury except in patients with a history of upper GI ulceration (Marlicz et al., 2014). Although the prostaglandin analog misoprostol has been shown to reduce the risk of both upper and small intestinal injuries associated with the use of NSAIDs (Fujimori et al., 2010), misoprostol causes abdominal pain, nausea or vomiting, or diarrhea in some patients (Taha et al., 2018), and poor tolerance limits clinical misoprostol usage, particularly for long term prophylaxis (Watanabe et al., 2008). Therefore, an agent promoting UGI and LGI mucosal healing would be valuable for patients who depend upon NSAIDs.

Gut mucosal healing is a complex process that involves restitution, proliferation, and angiogenesis, but its sine qua non is epithelial sheet migration, or restitution (Basson, 2017). Focal adhesion kinase (FAK), a 125 kDa non-receptor tyrosine kinase, is a key regulator of such cell motility (Walsh et al., 2008). Previous studies identified two commercially available small molecules that activate FAK in vitro (Raschka et al., 2018) and demonstrated that one of these molecules, ZINC40099027 not only stimulates Caco-2 cell monolayer wound closure in vitro at concentrations as low as 10 nM but also promotes mucosal wound healing in both ischemic and indomethacin-induced mouse intestinal injury models (Wang et al., 2019b). Moreover, this small molecule also ameliorates ongoing aspirin-induced gastric injury by activating FAK (Oncel et al., 2021). We recently described a library of novel FAK small-molecule activators that activate FAK and accelerate in vitro wound closure at concentrations as low as 100 pM while promoting small bowel mucosal wound healing in mice over three days without obvious toxicity (Wang et al., 2021). However, these FAK activators, like ZINC40099027 and other molecules so far studied, all required DMSO solubilization with attendant DMSO toxicity. We, therefore, synthesized and evaluated a new water-soluble compound, M64HCl, with promising drug-like properties and report here that it activates FAK, induces epithelial sheet migration in vitro, and stimulates gut mucosal wound healing in vivo.

2. Materials and methods

2.1. General information regarding the synthesis of M64/M64HCl

All reagents were purchased from commercial suppliers and used without further purification. All solvents used were reagent quality grade or anhydrous solvents. All reactions were performed under an inert atmosphere of nitrogen gas unless noted otherwise. ^{1}H NMR spectra were recorded on a Bruker Advance II (400 MHz). ^{1}H NMR data are reported as follows: chemical shift [multiplicity (s = singlet, d = doublet, t = triplet, q = quartet, dd = doublet of doublets, m = multiplet, s br = broad singlet), J = coupling constant(s) (Hz), integration]. Column chromatography was carried out employing Siliaflash silica gel (P60, 63–200 μm). Precoated silica gel plates F-254 were used for thin-layer analytical chromatography. All final compounds were purified to >95% purity as determined by LC/MS. Compounds were analyzed using a quadrupole/time of flight MS (G2S, Waters) coupled with a UPLC binary pump system (Acquity, Waters). Compounds were resolved on ACQUITY UPLC HSS T3 column (1.8 μM, 100 Å pore diameter, 2.1 × 150 mm; Waters) with a gradient of 0.1% formic acid in water (Solvent A) and acetonitrile with 0.1% formic acid (solvent B) at 0.3 mL/min. Percent B was increased from 1% to 75% over 2 min and then to 99% over 3 min. At 6 min, %B was returned to 1% over 1 min. Data were collected with the MS^E method, and MS was operated in sensitivity mode. Compounds were ionized with a positive electrospray ionization technique.

2.2. Synthesis of phenyl (2-morpholino-5-(trifluoromethyl)phenyl) carbamate

To a stirred solution of 2-morpholino-5-trifluoromethyl aniline (0.8 g, 3.2 mmol) in dry DCM (25 mL), under N_2 atmosphere at 0 °C, a solution of phenyl chloroformate (0.6 mL, 4.8 mmol) in dry DCM (5 mL) was added, followed by the addition of pyridine (0.65 mL, 8.10 mmol). The crude reaction was allowed to warm up at room temperature and stirred overnight. The crude reaction was concentrated *in vacuo* and product was purified by column chromatography using hexane: EtOAc (70:30) to afford 0.97 g (85% yield) of the pure product. ^{1}H NMR ($CDCl_3$, 400 MHz): δ 8.47 (s, 1H), 8.19 (s, 1H), 7.38 (d, J = 8.0 Hz, 2H), 7.32 (d, J = 8.0 Hz, 1H), 7.24 (d, J = 4.0 Hz, 2H), 7.19 (d, J = 8.0 Hz, 2H), 3.91 (t, J = 4.0 Hz, 4 H), 2.92 (t, J = 4.0 Hz, 4H). MS (ESI+) calculated for $C_{18}H_{17}F_3N_2O_3$ $[M+1]^+$: 367.3, observed: 367.3.

2.3. Synthesis of 1-(2-(dimethylamino)-2-(pyridin-4-yl)ethyl)-3-(2-morpholino-5-(trifluoromethyl)phenyl)urea (M64)

To a stirred solution of phenyl (2-morpholino-5-(trifluoromethyl) phenyl)carbamate (0.81 g, 2.21 mmol) in dry pyridine (5 mL), under N_2 atmosphere N^1,N^1-dimethyl-1-(pyridin-4-yl)ethane-1,2-diamine (0.44 g, 2.21 mmol) was added and the solution was heated at 80 °C for 16 h. The crude reaction was cooled down to room temperature and concentrated *in vacuo*. The residue was purified by column chromatography using DCM:EtOH (95:5) to afford 0.58 g (60% yield) of the pure product as an orange solid. ^{1}H NMR ($CDCl_3$, 400 MHZ): δ 8.45 (s, 1H), 8.32 (d, J = 8.0 Hz, 1H), 7.71 (s, 1H), 7.23–7.18 (m, 2H), 7.12 (d, J = 8.0 Hz, 1H), 6.26 (t, J = 8.0 Hz, 1H), 4.08–4.02 (m, 1H), 3.58–3.53 (m, 2H), 3.47–3.38 (m, 2H), 3.36-3-31 (m, 2H), 2.86–2.80 (m, 2H), 2.69–2.64 (m, 2H), 2.22 (s, 6H). ^{13}C NMR ($CDCl_3$, 400 MHZ): δ 155.14, 149.47, 149.23, 143.18, 134.85, 124.01, 120.29, 119.06, 116.17, 68.96, 66.74, 51.93, 42.97, 42.39. MS (ESI+) calculated for $C_{21}H_{26}F_3N_5O_2$ $[M+1]^+$: 438.20, observed: 438.20.

2.4. Synthesis of 1-(2-(dimethylamino)-2-(pyridin-4-yl)ethyl)-3-(2-morpholino-5-(trifluoromethyl)phenyl)urea hydrochloric salt (M64 HCl)

1-(2-(dimethylamino)-2-(pyridin-4-yl)ethyl)-3-(2-morpholino-5-(trifluoromethyl)phenyl)urea (0.438 g, 1.0 mmol) was stirred in 6 mL of a 3*N* solution of HCl in diethyl ether at room temperature overnight. The reaction mixture was concentrated *in vacuo* and lyophilized to obtain 0.47 g (quantitative yield) of the pure product as an orange solid. ^{1}H NMR (DMSO-d_6, 400 MHZ): δ 12.13 (s, br, 1H), 9.04 (d, J = 4.0 Hz, 2H), 8.32 (d, J = 8.0 Hz, 1H), 8.03 (d, J = 8.0 Hz, 2H), 7.25 (s, 2H), 4.87 (s, br, 1H), 4.08–4.04 (m, 1H), 3.85–3.80 (m, 5H), 2.98 (s, 2H), 2.74 (s, 6H), 2.62 (s, 2H). ^{13}C NMR (DMSO-d_6, 400 MHZ): δ 154.78, 150.74, 144.35, 143.49, 134.45, 127.54, 125.76, 124.41, 124.10, 123.10, 120.42, 118.55, 115.42, 67.20, 65.76, 51.28. MS (ESI+) calculated for $C_{21}H_{27}Cl_2F_3N_5O_2$ $[M+1]^+$: 474.18, observed: 438.20 – HCl.

2.5. Other chemicals and reagents

Dulbecco's modified Eagle's medium, Trypsin-EDTA, and Phospho-FAK (Tyr-397) recombinant rabbit monoclonal antibody (31H5L17 1:1000 dilution) were from Thermo Fisher (Waltham, MA). Antibodies to FAK-Tyr-397 (ab81298, 1:1000 dilution), Pyk2-Tyr-402 (ab4800, 1:1000 dilution), Src (ab16885, 1:1000 dilution), and Src-Tyr-419 (ab185617, 1:1000 dilution) were from Abcam (San Francisco, CA). Antibodies to total FAK (Anti-FAK, clone 4.47, 05–537, 1:1000 dilution) were from EMD Millipore, (Temecula, CA), and Pyk2 (3292 s, 1:1000 dilution) was from Cell Signaling Technology (Danvers, MA). Secondary antibodies anti-rabbit 800, anti-mouse 680, and anti-mouse 800 were from LI-COR (Lincoln, NE). Pepsin, >2000 U/mg protein was purchased from MP biomedicals (Irvine, CA). Indomethacin, misoprostol, hydroxyurea, potassium phosphate, sodium hydroxide, pancreatin from porcine pancreas,

and collagen I were purchased from Sigma Aldrich (St. Louis, MO). Glacial acetic acid was purchased from Fisher Chemical (Cat# A38S-500). Mini-Ames assay and in vitro ADME (absorption, distribution, metabolism, and excretion) studies were conducted by Pharmaron Inc (Beijing, China). Mouse serum chemistries were performed by the veterinary diagnostic laboratory at Michigan State University (Lansing, MI).

2.6. Cell culture

Human Caco-2 cells were purchased from ATCC (Manassas, VA) and cultured at 37 °C with 8% CO_2 in Dulbecco's modified Eagle medium with 4.5 g/l d-glucose, 4 mm glutamine, 1 mm sodium pyruvate, 100 U/ml penicillin, 100 μg/mL streptomycin, 10 μg/mL transferrin, 0.1 mm MEM non-essential amino acids solution, 10 mm HEPES pH 7.4, 3.7 g/l $NaHCO_3$ and supplemented with 10% fetal bovine serum. Human gastric epithelial AGS cells were maintained at 37 °C with 5% CO2 in Ham's F–12 K medium, with 100 U/mL penicillin, 100 μg/mL streptomycin, and 10% fetal bovine serum. IMR-90 lung fibroblast cells were cultured in EMEM media, with 10% FBS, 5% penicillin/streptomycin. SH-SY5Y neuronal cells were cultured in 1:1 EMEM: F12 media, with 10% FBS, 5% penicillin/streptomycin.

2.7. Western blotting

80–90% of confluent Caco-2 cells were seeded into cell culture plate pre-coated with 1% heat inactivated bovine serum albumin to prevent adhesion and avoid adhesion-associated background FAK activation. Suspended cells were then treated with H_2O control or M64HCl for 1 h before harvesting and lysis for Western blotting. Protein samples were then resolved by 10% SDS-PAGE, transferred onto nitrocellulose membranes, and blotted with antibody to Tyr-397-phosphorylated FAK. Antibody to total FAK served as a loading control.

2.8. Monolayer wound closure assay

Caco-2 cells were seeded at 80% confluence into collagen I coated cell culture plates. After 48–72 h, when the cells had reached 100% confluence, wounds were made in the monolayer with non-barrier autoclaved 200 μl tips. Cells were then treated with either M64HCl or H_2O vehicle control and cultured either without or with 4 mM hydroxyurea (HyU) for 24 h to prevent proliferation. Wound images were captured using an inverted light microscope (OLYMPUS CK2, Center Valley, PA) at 0 h and 24 h. Wound areas were measured with Image J software.

2.9. In vitro kinase assay

The FAK Kinase Enzyme System (V9301, Promega) was used for in vitro kinase enzymatic assay. The effect of M64HCl or M64 freebase on FAK activity was measured using a luminescent assay. The ADP-Glo™ Assay is a luminescent ADP detection assay that provides a homogeneous, high-throughput screening method to measure kinase activity by quantifying the amount of ADP produced during a kinase reaction. After the kinase reaction, the detection assay is performed in two steps; first, an equal volume of ADP-Glo™ Reagent is added to terminate the kinase reaction and deplete the remaining ATP. Second, the Detection Reagent is added to simultaneously convert ADP to ATP and allow the newly synthesized ATP to be measured using a luciferase/luciferin reaction. The light generated is measured using a luminometer. The luminescent signal positively correlates with kinase activity. Luminescence was measured using a Tecan Spark plate reader. (Grödig, Austria).

2.10. Cytotoxicity assay

IMR-90 lung fibroblast cells were plated in 96-well plates with 6500 cells per well, while SH-SY5Y neuronal cells were plated at 6000 cells per well. Twenty-four hours later, various concentrations of M64HCl were added to respective wells in 100 μl. After 48hrs for the IMR-90 cells, media was removed, plates were dip-washed in running water, and 60 μl of 0.5% crystal violet staining solution was added to each well including 2 wells that contained no cells for blanking. Plates were incubated for 20min on a bench rocker at the lowest speed. Plates were washed dipped in water 3–5x and air-dried overnight. Next, 150 μl of 100% methanol was added to each well, and plates were incubated at room temperature for 20min on a bench rocker with shaking. Optical density was measured at 570 nm with the Tecan Spark plate reader. Cytotoxicity for the SH-SY5Y was measured using the Promega CytoTox Assay per manufacturer's instructions (Promega, Madison, WI). (This kit was used since the SH-SY5Y cells are a mix of adherent and non-adherent cells.)

2.11. Animals and small intestine injury experimental models

Animal procedures were approved by the University of North Dakota Institutional Animal Care and Use Committee under protocols #2004–3, #2106–0003 and #2201–07.

Eight to ten week old C57Bl/6 J experimental mice were obtained from Jackson Laboratory (Bar Harbor, Maine) and housed in temperature-controlled rooms with a 12-h light/12-h dark cycle at 22–24 °C and 50–60% humidity. Ischemic ulcer induction was created by placing 75% acetic acid-saturated circular filter disks (3.14 mm^2) directly on the antimesenteric serosa for 15 s, without opening the bowel. In a second murine model, 17 mg/kg indomethacin was administered subcutaneously. Animals were then randomly assigned to receive either a continuous infusion of M64HCl (25 mg/kg/day) or a saline vehicle with osmotic pumps (model1007D, Alzet, Cupertino, CA) for four days. The osmotic pumps were surgically implanted subcutaneously at the same time as the acetic acid wound was made on the small intestine during the laparotomy or at the same time as the subcutaneous injection of indomethacin. On the day of sacrifice, mice were preliminarily anesthetized with isoflurane, blood was drawn by cardiac puncture. Next, cervical dislocation was performed to confirm euthanasia. Small intestine, liver, kidney, and other organs or tissues were excised for further study.

2.12. Bilateral functional nephrectomy

Thirteen-week-old C57Bl/6 J male and female mice were anesthetized using 4% isoflurane and maintained under anesthesia with 1–2% isoflurane. Following a laparotomy, a bilateral functional nephrectomy was performed by tying off the renal blood vessels leading to both kidneys with 3–0 surgical sutures. A subcutaneous injection of 25 mg/kg of M64HCl was administered. A paired non-surgical control mouse received a subcutaneous injection of 30 mg/kg M64HCl drug. The nephrectomized mouse remained under anesthesia for 2 h after M64HCl injection to minimize pain and suffering. A cardiac puncture was utilized to collect blood, then the liver and ileal mucosa were harvested. The non-surgical mouse was then anesthetized in order to collect blood by cardiac puncture and liver and ileal mucosa tissue. All mice had confirmed euthanasia by cervical dislocation. Liver and ileal mucosa were flash frozen with liquid nitrogen. Serum was collected after 2 centrifugations of 8000×*g* for 10 min. Tissue samples were homogenized in 300 μl of ice-cold water, and 20 μl of homogenate was mixed with 80 μl of 100% methanol.

2.13. UPLC-MS analysis for plasma, urine and tissue concentrations

Mouse samples (20 μL of tissue or feces homogenate, 10–20 μL of urine, or 20 μL of plasma or serum) were homogenized in methanol (80% final concentration). Precipitated proteins were separated by centrifugation at 2000×*g* for 10 min, and 10 μL of supernatant was injected onto the UPLC-MS/MS system for analysis.

UPLC separation was achieved using Waters Acquity I Class UPLC system (Waters, Milford, MA) on Waters ACQUITY UPLC HSS T3 column (1.8 μM, 100 Å pore diameter, 2.1 × 150 mm; Waters) with an ACQUITY

UPLC HSS T3 precolumn (1.8 μM, 100 Å pore diameter, 2.1 × 5 mm; Waters) heated at 55 °C. We used a linear gradient of solvents A (0.1% formic acid in water) and B (0.1% formic acid in acetonitrile) at 0.3 mL/min. At 1 min of separation, initial %B was increased from 1% to 25% during 1 min, and at 2.1 min – to 90% during 1.9 min. At 5 min, solvent B was returned to 1% and allowed 4 min for equilibration between injections.

MS/MS analysis was performed on Waters Xevo TQ-S triple quadrupole mass spectrometer (Waters, Milford, MA) using multiple reaction monitoring mode. The MS was operated in a positive ESI mode. The following mass transitions (with collision energies (CE) indicated in parentheses, V) were used: 438.2/273.1 (25) for quantification; 438.2/192.1 (20) and 438.2/149.2 (24) for analyte confirmation.

The UPLC-MS/MS system was controlled by MassLynx V4.1. Quantification was performed against an M64HCl external standard using a generated response curve.

2.14. Histology and immunohistochemistry

Mouse kidney and liver tissues were fixed in neutral-buffered 10% formalin solution for 48 h, then processed and embedded in paraffin. Five-micron sections were stained with hematoxylin and eosin. Small intestine ulcer tissue sections were prepared for immunostaining as previously described (Wang et al., 2019b). Intensity of immunoreactivity for FAK phosphorylation in the migrating epithelium at the edge of the ulcer was scored between 0 and 4, with 0 being the least amount of detectable positive staining and 4 being the highest positive staining. Assessment was performed independently by two observers blinded to the group assignments.

2.15. Statistical analysis

Data are expressed as mean ± standard error and were analyzed using GraphPad prism version 9. Q test was applied to remove outliers. Results were compared by Student's unpaired *t*-test as appropriate seeking 95% confidence. For comparing more than two sets of data, ordinary one-way ANOVA was performed. A *p*-value of <0.05 was considered statistically significant.

3. Results

3.1. M64/M64HCl structure and quality control

Fig. 1 shows the structures of 1-(2-(dimethylamino)-2-(pyridin-4-yl) ethyl)-3-(2-morpholino-5-(trifluoromethyl)phenyl)urea (M64, Fig. 1a) and 1-(2-(dimethylamino)-2-(pyridin-4-yl)ethyl)-3-(2-morpholino-5-(trifluoromethyl)phenyl)urea hydrochloric salt (M64HCl, Fig. 1b). Purity of M64 was 94% (Fig. 1c). Purity of M64HCl was 95.8% (Fig. 1d).

3.2. M64HCl activates FAK in Caco-2 cells

Suspended Caco-2 cells treated with M64HCl activated FAK-Tyr397 phosphorylation at 100 pM and 1 nM by 8.7 ± 3.0%, 9.1 ± 3.9% respectively (Fig. 2a, n = 4, $*p < 0.05$). Caco-2 cells were treated with M64HCl at 10–1000 nM at 37 °C for 1 h increased FAK-Tyr 397 phosphorylation in comparison to H2O controls by 20.2 ± 7.4%, 25.3 ± 7.8% and 28.4 ± 9.3% respectively (Fig. 2b n = 6, $*p < 0.05$). The FAK activation effect at 100 nM was confirmed by adding ZN40099027 as a positive control (Fig. 2c n = 8, $*p < 0.05$). We then tested FAK activation in human gastric epithelial AGS cells. M64HCl increased FAK-Tyr-397 phosphorylation in comparison to H2O controls by 20.2 ± 7.4% at 100 nM (Fig. 2d). Interestingly, the non-salt molecule M64 did not activate FAK at 10–1000 nM concentration (Fig. 3a). In contrast, M64HCl did not activate the FAK paralog, proline-rich tyrosine kinase 2 (Pyk2), as measured by phosphorylation of Pyk2-Tyr-402 even at 1000 nM (Fig. 3b). M64HCl also did not activate the non-receptor protein tyrosine kinase Src, as assessed by phosphorylation of Src-Tyr-419. (Fig. 3c).

3.3. M64HCl has promising drug-like properties

Solubility of M64HCl in PBS buffer, pH 7.4 was 289.29 μM. No degradation was observed in either gastric simulated fluid (pH = 1.2) (Fig. 4a) or intestinal simulated fluid (pH = 6.8) (Fig. 4b) for up to 4 h. Mini-Ames assay was negative. M64HCI did not induce a ≥2-fold increase (for tester strain TA98, TA100 and WP2 uvrA (pKM 101)) or ≥3-fold increase (for tester strain TA1535 and TA1537) of revertant colonies at any dose levels when compared to the concurrent negative/solvent control. No dose related increase of revertant colonies was observed. IC_{50} of CYP2C9, CYP2C19, CYP2D6 and CYP3A4 by M64HCl in human liver microsomes were 1.25 μM, 3.98 μM, 15.41 μM, 0.44 μM respectively (Fig. 5. The potential inhibitory effect of M64HCl on human Ether-à-go-go related gene (hERG) channel was evaluated by using manual patch-clamp system. IC_{50} was greater than 30 μM, suggested that M64HCl ranked as a weak inhibitor on hERG channel. The distribution coefficient (Log D) in octanol/PBS was 2.87. Protein binding studies in human plasma demonstrated that the molecule was 91.4% bound, with 116.7% recovery and 88.6% stability at 6 h.

3.4. M64HCl stimulates Caco-2 cell monolayer wound closure

Compared with the H_2O vehicle control, incubation with 10 nM or 100 nM M64HCl for 24 h stimulated Caco-2 epithelial wound closure by 13.0 ± 0.8% and 24.3 ± 0.9% respectively (Fig 6a,c, n = 16, pooled from 4 separate studies, $*p < 0.05$). Even when proliferation was blocked by 4

Fig. 1. (a) Structure of M64. (b) Structure of M64HCl. (c) M64 purity by LC/MS. (d) M64HCl purity by LC/MS.

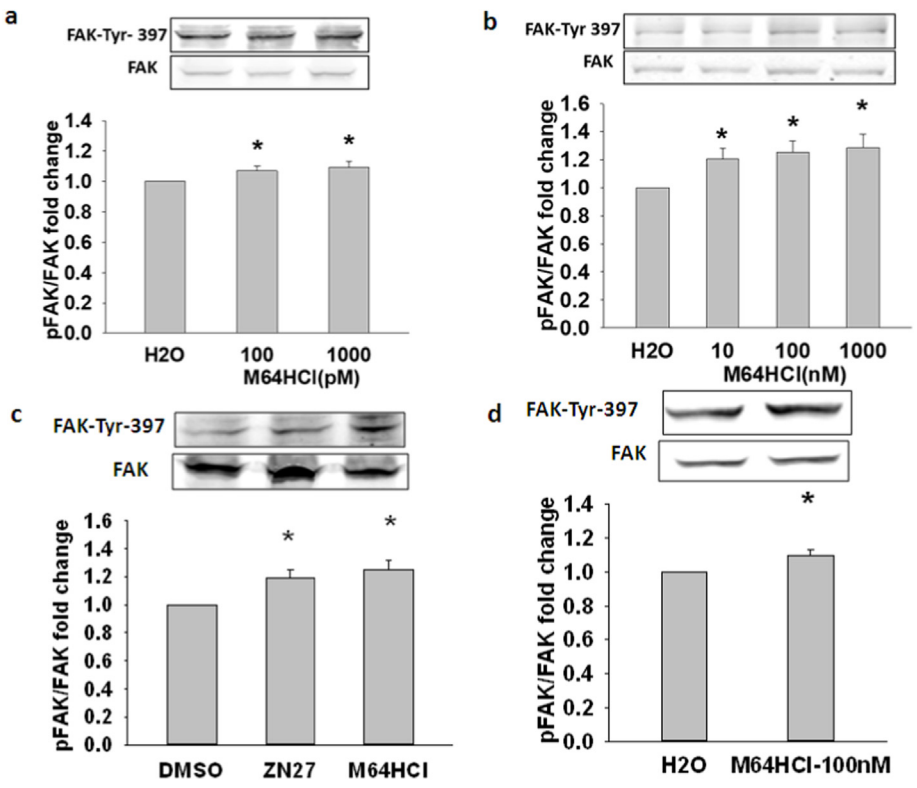

Fig. 2. The effect of M64HCl on phosphorylation of FAK-Tyr-397 in human Caco-2 cells. (a) Representative blots and Tyr-397/FAK fold change in Caco-2 cells in suspension at 100pM and 1000pM concentration (n = 4, $*p < 0.05$). (b) Representative blots and Tyr-397/FAK fold change in Caco-2 cells in suspension at 0–1000 nM after treatment with M64HCl (n = 6, $*p < 0.05$). (c) ZN40099027 as a positive control activates FAK at 100 nM (n = 8, $p < 0.05$). (d) Representative blots and Tyr-397/FAK fold change in AGS cells treated with M64HCl at 100 nM.

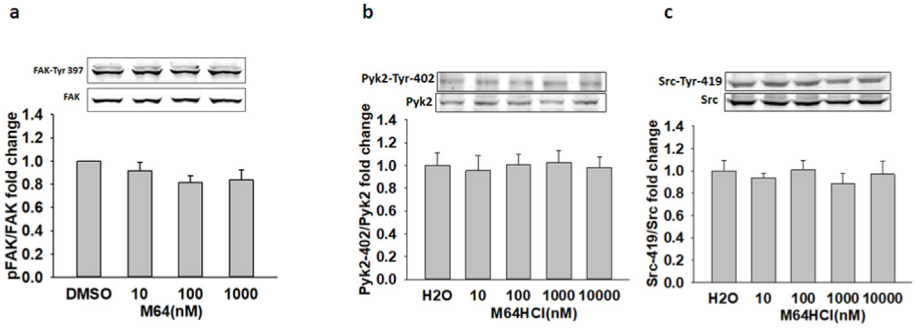

Fig. 3. (a) The non-salt version of the molecule M64 does not activate FAK at 10–1000 nM. (b) M64HCl at 10–10,000 nM does not stimulate the phosphorylation of Pyk2 at Tyr-402. (n = 4), or of Src (c) at Tyr-419 (n = 4).

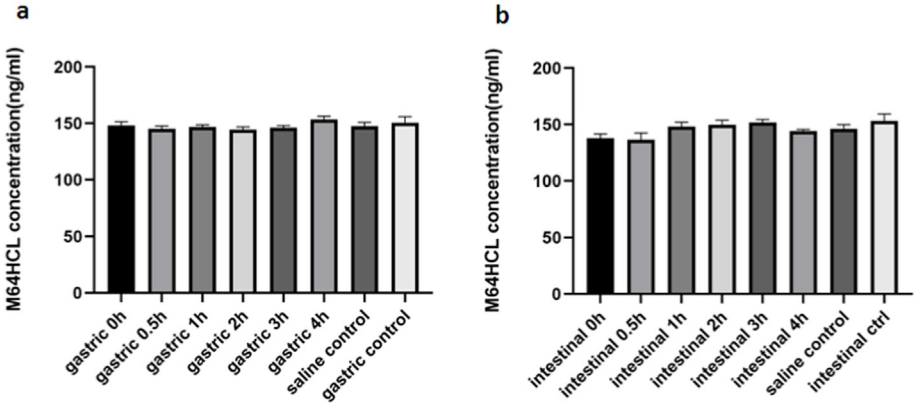

Fig. 4. M64HCl stability in simulated fluid. (a) M64HCl concentration in gastric simulated fluid at 0–4 h compared to stability in saline. (b)) M64HCl concentration in intestinal simulated fluid at 0–4 h compared to saline.

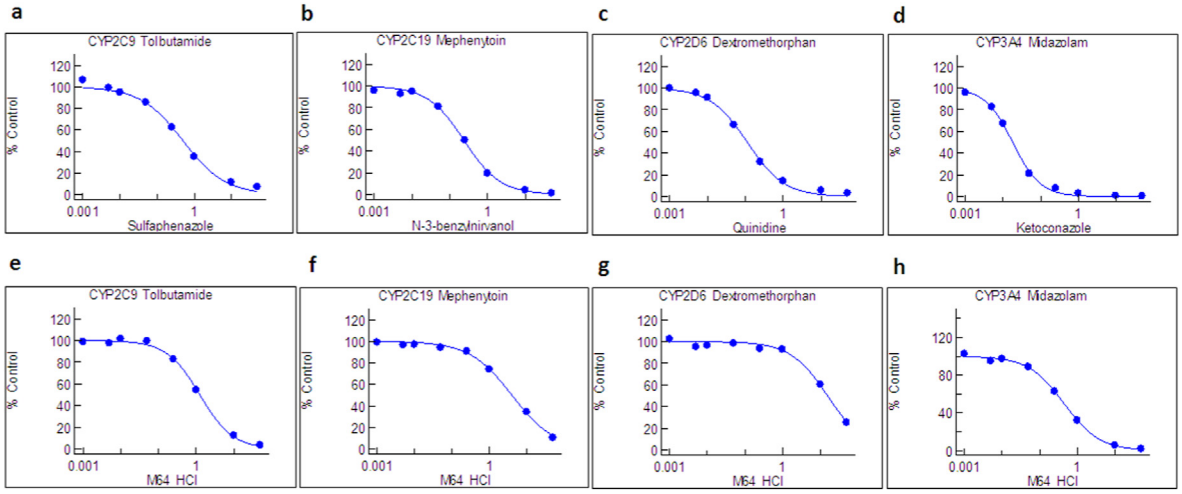

Fig. 5. Inhibition of CYP2C9, CYP2C19, CYP2D6 and CYP3A4 by M64HCl in vitro in human liver microsomes.

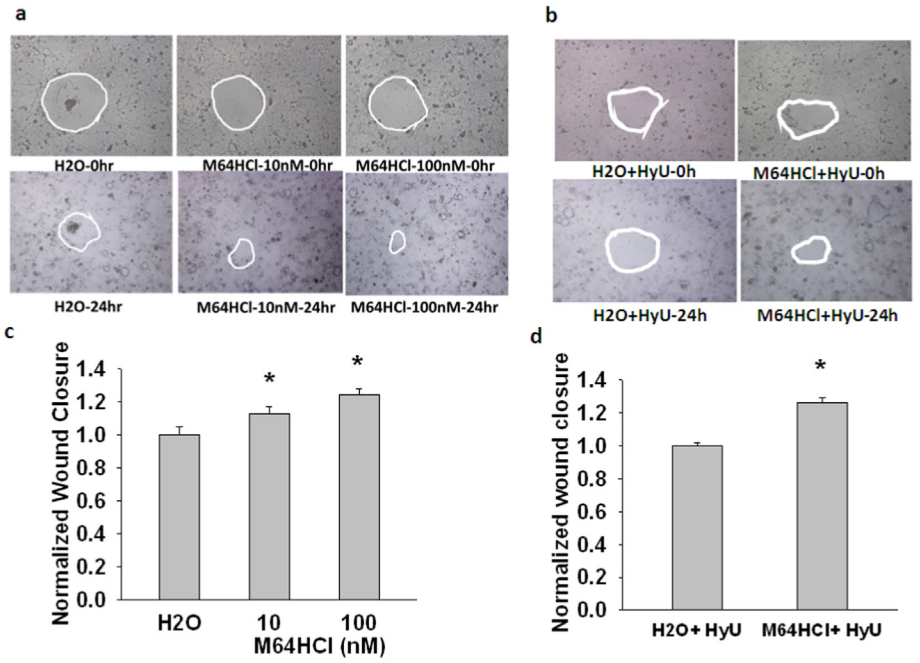

Fig. 6. The effect of M64HCl on Caco-2 cell monolayer wound closure. (a) Typical wound images treated with H2O or M64HCl at 10 nM or 100 nM. Images were taken at 0 and 24 h after wounding. (b) Typical wound images treated with H2O or M64HCl at 10 nM in the presence of 4 mM hydroxyurea. (c) 10 nM or 100 nM M64HCl accelerates wound closure in Caco-2 monolayers. (n = 16, pooled from 4 separate studies, $*p < 0.05$). (d) M64HCl enhances Caco-2 cell monolayer wound even when proliferation is blocked by 4 mM hydroxyurea (n = 16, $*p < 0.05$).

mM hydroxyurea, M64HCl still accelerated circular monolayer wound closure in comparison to H_2O controls (Fig. 6b,d, n = 16, pooled from 4 separate studies, $*p < 0.05$). These results suggested that M64HCl not only activates FAK but also stimulates epithelial sheet migration.

3.5. M64HCl interacts directly with the FAK kinase domain to activate FAK

When purified full-length FAK (125 kDa) or FAK kinase domain (35 kDa) were incubated for 30 min in the presence of ATP without and with 10 nM M64HCl, we observed a significantly increased kinase activity for both full-length FAK (Fig. 7a, 1.58 ± 0.04, n = 4, $*p < 0.05$) and its kinase domain (Fig.s. 7b and 1.24 ± 0.05, n = 4, $***p < 0.01$) compared to control. To determine the optimal activating concentration of M64HCl in vitro, we used this same luminescent ADP detection system with the purified FAK kinase domain over a range of M64HCl concentrations. M64HCl dose-dependently activates the FAK kinase domain compared to the non-salt M64 molecule (Fig. 7c). M64HCl increases the Vmax of ATP-binding in comparison to H2O control (Fig. 7d). These results suggest that M64HCl is a direct and highly potent activator of FAK.

3.6. M64HCl promotes mucosal healing after mouse intestinal mucosal injury

We first administered 2 mg/kg intraperitoneally to C57BL/6 J mice and measured plasma M64HCl concentration over 12 h. M64HCl plasma level peaked 1 h after intraperitoneal injection and decreased substantially by 2hrs (Fig. 8a). Next, we administered M64HCl 10 mg/kg by gavage to mice and found a similar pharmacokinetic pattern (Fig. 8b). We next studied in vivo intestinal epithelial mucosal healing in response to M64HCl. To maintain a stable plasma concentration, we performed continuous 25 mg/kg/day M64HCl infusion by osmotic minipumps for 4 days. Ischemic jejunal mucosal ulcers were created by application of acetic-acid-soaked discs of filter paper for 15 s to the serosa of the bowel. Mice receiving M64HCl for four days after the procedure exhibited smaller ulcers than those that had received the saline control (Fig. 8 c-8d.

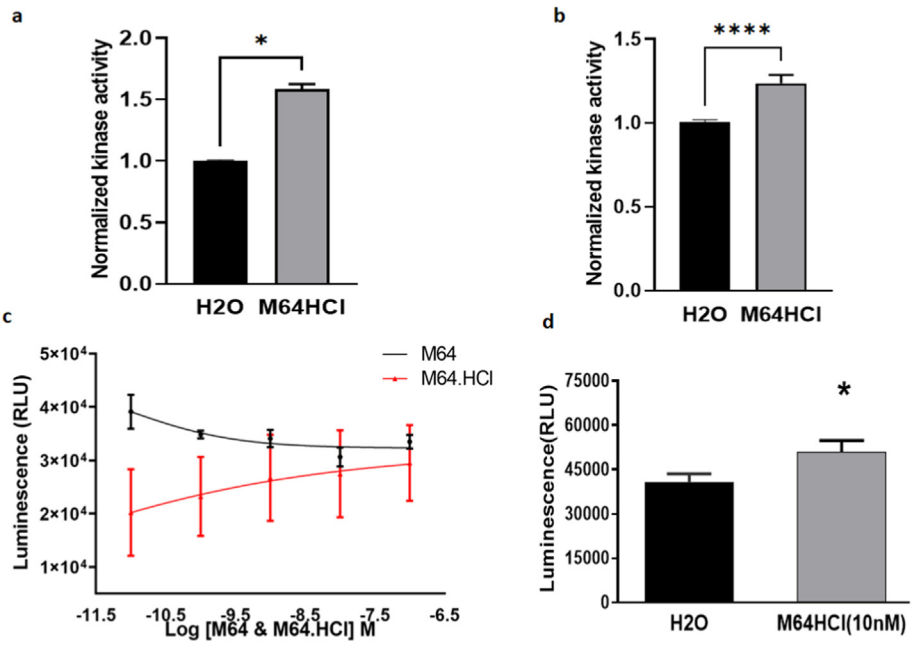

Fig. 7. M64HCl interacts with the FAK kinase domain. (a) M64HCl stimulates the conversion of ATP to ADP by highly purified full-length 125 kDa human FAK in an in vitro kinase assay 2 independent experiments with 4 replicates in each experiment, $*p < 0.05$). (b) M64HCl binding stimulates the conversion of ATP to ADP by the 35 kDa FAK kinase domain (Figure represents pooled data from 3 experiments with 4 replicates in each experiment, n = 2, $*p < 0.01$). (c) M64HCl dose dependently activates the FAK kinase domain compared to the non-salt M64 molecule. (d) M64HCl increases the Vmax of ATP-binding vs. H2O control (n = 6, $*p < 0.05$).

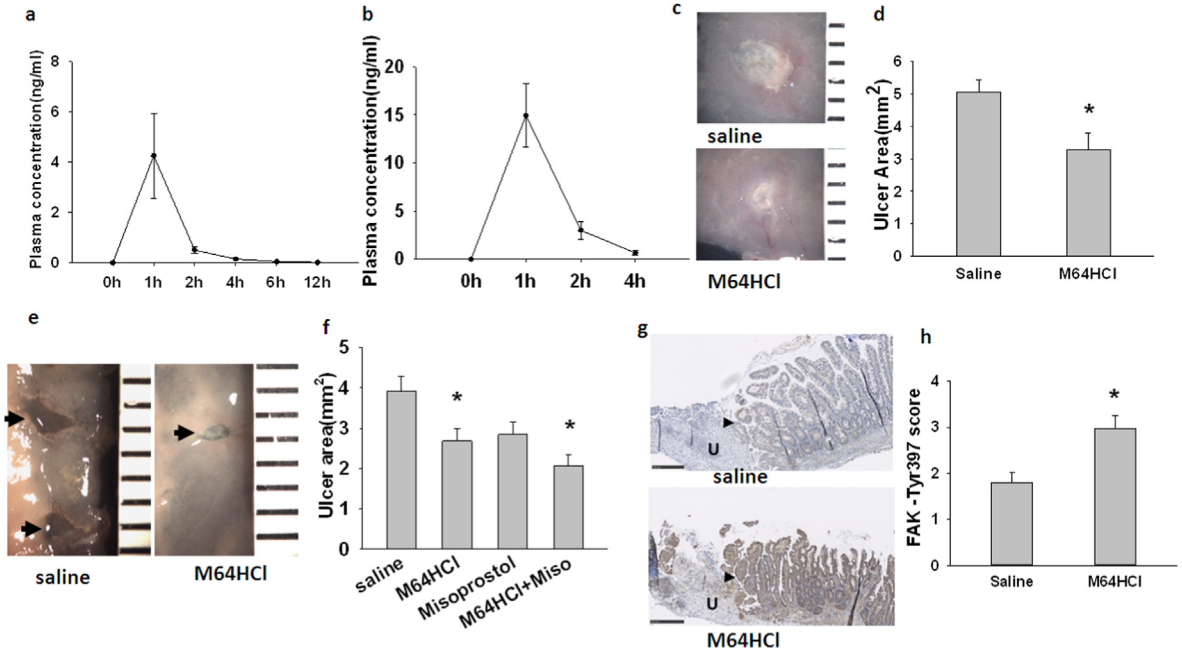

Fig. 8. M64HCl promotes mucosal healing in two murine small intestinal injury models. (a) M64HCl plasma concentration 0–12 h after a single intraperitoneal injection of 2 mg/kg in mice. (b) M64HCl plasma concentration after 10 mg/kg gavage administration. (c) Representative images of jejunal ischemic ulcers in saline-treated mice and M64HCl-treated mice 4 days after ulcer-induction. (d) Ischemic ulcer area after 4 days of M64HCl continuous infusion or saline treatment (3.28 ± 0.50 vs. 5.06 ± 0.37 mm^2, n = 10, $*p < 0.05$). (e) Representative images of indomethacin induced small intestine ulcers from saline-treated mice and M64HCl-treated mice. (f) Total ulcer size in indomethacin induced small intestinal injury treated with saline control, M64HCl, misoprostol or M64HCl plus misoprostol (3.92 ± 0.37 mm^2 in saline vehicle vs. 2.69 ± 0.29 mm^2 in M64HCl vs. 2.84 ± 0.32 mm^2 in misoprostol only vs.2.07 ± 0.29 mm^2 in synergistic treatment, n = 12, $*p < 0.05$). (g) Representative immunohistochemical images of FAK-397 phosphorylation in epithelium at the edge of the ulcer bed from saline control or M64HCl-treated mice. Arrows indicate epithelium at the edge of the ulcer. (h) Blinded phosphor-FAK immunoreactivity scores are increased in M64HCL-treated ulcers vs. saline-treated ulcers (n = 9, $*p < 0.05$).

3.28 ± 0.50 vs. 5.06 ± 0.37 mm^2, n = 10, $*p < 0.05$). In a second in vivo mouse model, mice were given 17 mg/kg indomethacin subcutaneously to induce small intestine injury and then randomized to receive saline control, 25 mg/kg/day M64HCl, 800 μg/kg/day of misoprostol, or M64HCl plus misoprostol for 4 days. By day 4, multiple ulcerative lesions were seen throughout the small intestine. M64HCl reduced the total small intestine ulcer area to 2.69 ± 0.29 mm^2 compared to 3.92 ± 0.37 mm^2 in vehicle-treated mice (Fig. 8e $p^*<0.05$). Misoprostol treatment alone reduced ulcer area to 2.84 ± 0.32 mm^2. Total ulcer area in the intestines of mice receiving both M64HCl and misoprostol was 2.07 ±

0.29 mm^2, also lower than the saline control (Fig. 8f $p^*<0.05$). Blinded immunohistochemical assessment demonstrated higher immunoreactivity for phosphorylated FAK in the epithelium at the edge of M64HCL-treated ulcers vs. saline-treated ulcers (Fig. 8g and h,2.97 ± 0.28 vs 1.81 ± 0.21 on a 1 to 4 scale, n = 9, $p < 0.05$). The plasma M64HCl concentration was 58 ng ± 11.2 ng/mL at the time of sacrifice, approximately equivalent to 122.4 ± 23.5 nM.

3.7. Four days of M64HCl continuous infusion treatment does not affect murine renal or hepatic function

Plasma creatinine and alanine aminotransferase (ALT) levels were measured as indicators of renal and hepatic function in both ulcer models. (Table 1). Plasma creatinine remained within the normal range in mice without any statistical difference between saline or M64HCl groups in both ischemic ulcer and indomethacin induced-injury models. Plasma ALT concentration was higher than normal in both saline-treated mice and M64HCl-treated mice in both ulcer models, but the M64HCl treated mice did not show higher levels than those treated with the saline vehicle. Renal histology was normal when sacrifice. Each model resulted in some hepatic inflammatory changes but these appeared similar among M64HCl-treated mice and controls.

3.8. M64HCl treatment does not cause obvious behavioral changes or increase weight loss in small intestinal injury models

We saw no fur ruffling or behavioral abnormalities. Although all mice lost weight with the ischemic ulcer model, we did not observe more weight loss in the M64HCl-treated mice. Weight loss was 4.7 ± 1.1% for controls with saline vs. 4.6 ± 0.7% for M64HCl-treated mice in the ischemic ulcer model. After indomethacin-induced small bowel injury, the average weight loss in saline-treated, M64HCl-treated, misoprostol-treated, and combination-treated mice was 6.08 ± 0.72%, 4.92 ± 0.84%, 5.53 ± 1.18%, and 4.70 ± 1.0% respectively.

3.9. M64HCl tissue distribution

To further understand M64HCl tissue distribution and metabolization, we examined M64HCl concentration in mouse tissues after four days continuous minipump infusion at 25 mg/kg/day. M64HCl appeared concentrated in the kidney, gastric mucosa, and intestinal mucosa (Fig. 9a). The concentration of M64HCl in the urine was 300.84 ± 55.27 ng/mL, approximately six-fold higher than that in plasma, suggesting that M64HCl is concentrated and excreted in the urine (Fig. 9b). To further confirm that M64HCl is largely excreted by the kidneys, we performed a bilateral functional nephrectomy to ablate all renal clearance, and then examined drug levels in the serum, liver, and ileal mucosa. We observed a significant increase in M64HCl within the ileal mucosa, liver, and serum 2 h after drug administration in functional nephrectomized mice compared to non-surgical control mice (Fig. 9c). In a separate experiment, we administered a 5 mg/kg single dose of M64HCl intraperitoneally and then measured plasma and brain concentrations at 30 min and 2 h. Thirty minutes after injection, the brain/plasma ratio was 0.06 ± 0.01 while at 2 h, the brain/plasma ratio increased to 0.26 ± 0.07, suggesting some ability of M64HCl to cross the blood-brain barrier over time (Fig. 9d).

3.10. M64HCl exhibits little toxicity at higher than FAK-activating concentrations

IMR-90 human pulmonary fibroblasts and SH-SY5Y human neuronal cells were treated with M64HCl at 0–1000 μM. The toxic IC_{50} for the M64HCl was 1 mM in the IMR-90 cells (Fig. 10a) and 200 μM for the SH-SY5Y cells (Fig. 10b), substantially higher than the 100 pM threshold concentration that activates FAK or even the 122 nM plasma concentration we achieved in our mouse studies.

We attempted to ascertain the highest single tolerated dose of M64HCl in vivo. Mice were given single intraperitoneal doses of M64HCl at 120 mg/kg, 180 mg/kg and 240 mg/kg (4-fold, 6-fold, and 8-fold higher dosing in comparison to mouse intestinal mucosal injury models) were healthy 14 days later, while mice receiving 360 mg/kg were sick and uncomfortable after 48hrs injection and were euthanized. Serum chemistries at 120 mg/kg, 180 mg/kg and 240 mg/kg were similar. Hepatotoxicity was seen at 360 mg/kg (Table 2).

4. Discussion

There is a critical need for a new agent that directly promotes both upper and lower GI healing and might be used to ameliorate ongoing mucosal injury associated with chronic NSAID use. M64HCl specifically activates FAK and promotes epithelial sheet migration both in vitro and in vivo. It has drug-like properties, does not appear toxic, at least in the short term, until levels 1000x higher than therapeutic are achieved, and is enterally absorbed.

Mucosal healing balances epithelial migration and proliferation to resurface the injured gut against continual injury (Basson, 2017). NSAIDs injure UGI mucosa by inhibiting cyclo-oxygenase, the primary enzyme responsible for prostaglandin synthesis. This impairs mucosal blood flow, mucus and bicarbonate secretion, and platelet aggregation. (Wallace, 2001; Wallace, 2008, Iwamoto et al., 2013). COX-2 selective inhibitors produce fewer upper gastrointestinal complications (Lanas, García-Rodríguez et al. 2006; Rostom et al., 2007), and either COX-2 selective agents or the combination of NSAIDs with a proton pump inhibitor have been recommended to prevent NSAID-induced upper GI ulceration (Kavitt et al., 2019) and to reduce the risk of recurrent UGI bleeding in patients at high risk of both gastrointestinal and cardiovascular events who require aspirin and NSAID for cardiovascular and anti-inflammatory therapies (Chan et al., 2017b). However, the symptoms of patients treated with COX-2 inhibitors for more than three months were no different from those of patients treated with traditional NSAIDs (Maiden et al., 2007; Sugimori et al., 2008) and a recent systematic review concluded that selective COX-2 inhibitors increase the risk of myocardial infarction and other cardiovascular events (Gøtzsche, 2010). PPIs that inhibit the hydrogen pump in the parietal cell directly, or H2 receptor antagonists that block the histamine receptor on parietal cells thereby reducing hydrogen ion release have been recommended to co-prescribed with NSAIDs to prevent the side effects of UGI (Sugano et al., 2014; Chan et al., 2017a; Chen et al., 2017; Szabó et al., 2017; Kamada et al., 2021). However, both animal studies and clinical evidence demonstrate that use of PPIs or H2 receptor antagonists dramatically worsens distal intestinal damage (Satoh et al., 2012; Tai and McAlindon, 2018), increase lower gastrointestinal bleeding risk (Lanas et al., 2015; Miyake et al., 2015; Lué and Lanas, 2016), and exacerbate NSAID-induced small intestinal ulceration (Wallace et al., 2011). The underlying mechanism of this worsening has been linked to marked increases in bile cytotoxicity when

Table 1
Mouse plasma creatinine and ALT concentrations after receiving saline or M64HCl 30 mg/kg/day for four days.

	Normal Range	Ischemic ulcer model		Indomethacin model	
		Saline (n = 6)	M64HCl(n = 6)	Saline (n = 6)	M64HCl(n = 6)
Plasma creatinine	0.06–16 mg/dl	0.11 ± 0.013	0.12 ± 0.023	0.14 ± 0.03	0.10 ± 0.02
Plasma ALT	0.67–3.76 ng/mL	13.08 ± 2.03	13.15 ± 1.82	4.58 ± 0.47	5.02 ± 0.73

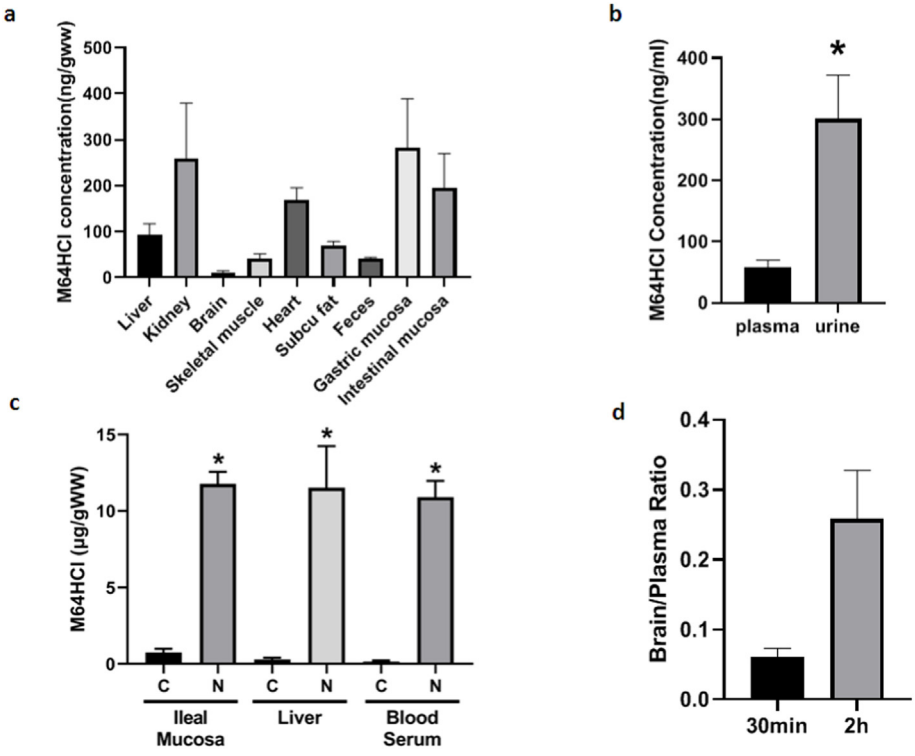

Fig. 9. M64HCl tissue distribution. (a) M64HCl concentration in tissues after a four day continuous osmotic mini-pump infusion at 30 mg/kg/day. (b) M64HCl levels in mouse plasma vs. urine after a 4 day infusion at 30 mg/kg/day (n = 8, $*p < 0.05$). (c) M64HCl excretion was blocked by a bilateral functional nephrectomy. M64HCl drug levels were measured by LC-MS 2 h after bilateral functional nephrectomy and a subcutaneous injection of 30 mg/kg of M64HCl. C = non-surgical controls, N = nephrectomy (n = 2, $*p < 0.05$). (d) M64HCl in brain vs plasma 30 min or 2 h after 5 mg/kg was administered intraperitoneally.

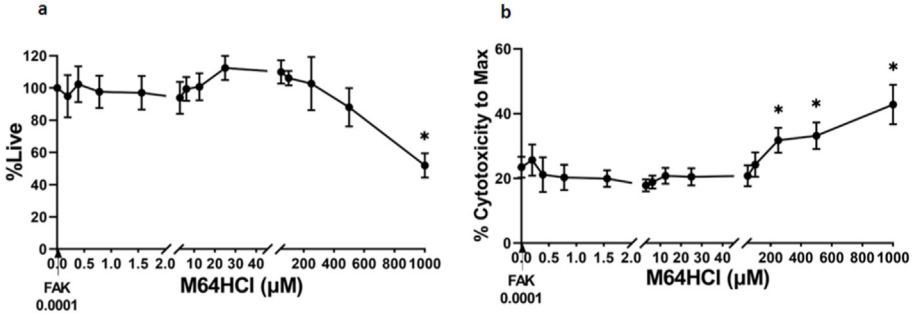

Fig. 10. The toxic IC50 for M64HCl exceeds FAK activating concentrations 10^7-fold. (a) % live IMR-90 cells after 48 h M64HCl exposure, analyzed by crystal violet cytotoxicity assay. Lower % numbers mean cell death. (b) % cytotoxicity to max LDH release in SH-SY5Y cells, analyzed via Promega CytoTox Assay. Higher % numbers mean cell death. X-axes are split from 2 to 10 and 40–50. FAK activation threshold is labelled "FAK", in µM below, and with a dotted red line. N = 8–9 for IMR-90 cells, N = 6–8 for SH-SY5Y cells; $*p < 0.05$.

complexed with NSAIDs and to changes in the intestinal microbiota associated with gastric acid neutralization (Syer et al., 2015). The prostaglandin analog misoprostol elevates prostaglandin levels in the serum and small intestinal mucosa, promoting mucosal defense by increasing blood flow and enhancing mucus and bicarbonate secretion (Teutsch et al., 2021). While misoprostol can heal small intestine ulcers in aspirin users (Park et al., 2011; Kyaw et al., 2018) a recent review deemed its protective ability insufficient (Watanabe et al., 2020). Moreover, misoprostol can be poorly tolerated due to side effects including nausea, vomiting, diarrhea, and abdominal pain (Rostom et al., 2002; Taha et al., 2018), and is not conducive to chronic prophylaxis.

FAK regulates many of the cellular processes that are critical for epithelial homeostasis and restitution, including cell migration, proliferation, and survival. FAK is both a scaffold protein and a non-receptor tyrosine kinase that is essential during development and plays key functions in tissue repair and wound healing (Ashton et al., 2010; Owen et al., 2011; Burridge, 2017). FAK activation is critical for mucosal healing (Alam et al., 2014; Khan et al., 2014). FAK activation begins with a conformational change releasing the FAK kinase domain from the (inhibitory) FAK FERM domain. This frees the FAK kinase domain to autophosphorylate FAK at Tyr-397(Lietha et al., 2007). The interfaces responsible for initial dimerization and membrane attachment are essential for FAK autophosphorylation (Acebrón et al., 2020). Activated FAK is decreased at the edge of intestinal epithelial monolayer wounds in vitro (Basson et al., 2006) and around human gastric and colonic ulcers in vivo (Walsh et al., 2008), which makes FAK an attractive target for pharmacotherapy to promote gastrointestinal mucosal wound healing. Our investigation of FAK activators begin with a search to block an AKT1-FAK interaction that promotes metastasis (Thamilselvan et al., 2007; Craig et al., 2008; Wang and Basson, 2011). A FAK FERM-domain-derived 7-mer amino acid peptide prevents this interaction (Zeng et al., 2017). We therefore sought to mimic this FAK subdomain's structure by in silico screening existing small molecules based on assumptions about the subdomain's tertiary conformation (Raschka et al., 2018). A virtual screen of the ZINC Database yielded molecules based on an active FAK mutant peptide that reduced cancer cell adhesiveness. However, two molecules based on the homologous wild type FAK sequence turned out to activate FAK. We then engaged in study of a series of additional related molecules and identified four additional that stimulate FAK phosphorylation at remarkably low concentrations (Wang et al., 2021). However, all of those molecules so far been studied had required DMSO solubilization with attendant DMSO toxicity. In further exploration, we, therefore, synthesized and evaluated this new water-soluble compound, M64HCl. Like the previous molecules we have

Table 2
Mouse serum chemistries after a single dose injection of M64HCl.

Animal ID	Urea Nitrogen (mg/dL)	Creatinine (mg/dL)	Sodium (mmol/L)	Potassium (mmol/L)	Chloride (mmol/L)	TCO2 (mmol/L)	Na/K Ratio	Anion Gap (mmol/L)	Osmolarity Calc (mmol/L)	Calcium (mg/dL)
120 mg/kg	27	0.2	145	7.3	110	19	20	23	314	8.6
180 mg/kg	20	0.2	145	6.2	111	21	23	19	311	8.6
240 mg/kg	26	0.2	144	5.7	111	19	25	20	310	8.6
360 mg/kg	175	1	144	9.1	114	12	16	27	365	9.1

Animal ID	**Phosphorus (mg/dL)**	**Magnesium (mg/dL)**	**Iron (ug/dL)**	**Total Protein (g/dL)**	**Albumin (g/dL)**	**Globulin Calc (g/dL)**	**Glucose (mg/dL)**	**Amylase (U/L)**	**Total Bili (mg/dL)**	**Direct Bili (mg/dL)**
120 mg/kg	7.6	2.6	162	4.5	2.7	1.8	254	559	0.2	0
180 mg/kg	8	2.6	124	4.3	2.8	1.5	242	373	0.2	0
240 mg/kg	8	2.5	139	4.3	2.7	1.6	236	908	0.2	0
360 mg/kg	QNS	6.1	137	3.5	2.3	1.2	259	QNS	0.4	0

Animal ID	**Indirect Bili (mg/dL)**	**ALP (U/L)**	**GGT (U/L)**	**ALT (U/L)**	**AST (U/L)**	**CK (U/L)**	**Chol (mg/dL)**	**Hemolysis Chem**	**Icterus Chem**	**Lipemia Chem**
120 mg/kg	0.2	72	<3	106	628	8986	72	Normal	Normal	Normal
180 mg/kg	0.2	63	<3	80	539	8140	76	Normal	Normal	Normal
240 mg/kg	0.2	75	<3	96	684	8839	68	Normal	Normal	Normal
360 mg/kg	0.4	329	7	721	1738	QNS	35	slight	Normal	Normal

QNS: need to go around again to be diluted because it was quite high.

studied in the series, M64HCl seems likely to mimic this FAK subsequence and thus bind to FAK itself, unfolding the molecule and permitting its autoactivation.

We previously reported that the FAK activator ZN40099027 enhances FAK activity via interaction with the FAK kinase domain to increase the Vmax of FAK for ATP(RashmiVomhof-DeKrey et al., 2021). ZN40099027 at 10 nM activates FAK by 14.8% in suspended Caco-2 cells (Wang et al., 2019b). This new molecule, M64HCl may be more potent in that it activates FAK at concentrations as low as 100 pM, and produces a 20.2% activation at 10 nM. The effects of M64HCl seem dose-responsive, but non-linear at higher concentrations, rather plateauing at 20–30% activation. Although this may seem like a limited level of activation, we and others have previously studied the significance of increases (Craig et al., 2008; Xie et al., 2018; Li et al., 2019) and decreases (Shiratsuchi and Basson, 2004, Usechak et al., 2008; Wang et al., 2019a) of similar magnitude in FAK phosphorylation in other contexts. FAK activation is at the top of a signal cascade that amplifies its effects to produce very real biological consequences. Indeed, our present results suggest that this modest effect stimulates Caco-2 cell monolayer wound closure while our in vivo studies clearly demonstrate that M64HCl promotes intestinal mucosal healing in two animal models of small intestinal injury.

M64HCl does not activate either Pyk2, the kinase most closely related to FAK, or Src, the other canonical major non-receptor tyrosine kinase within the focal adhesion complex even at 10 μM, a 10,000-fold higher concentration than that required to activate FAK. We would expect (and indeed have previously reported for the FAK activating ZN27 (Oncel and Basson, 2022) that other kinases downstream of FAK will also be activated in response to FAK activation. Whether M64HCl directly binds to some other kinase independently of its ability to activate FAK may be theoretically less likely because it does not activate Pyk2, but remains a possibility for future study. M64HCl appears to promote epithelial sheet migration directly in vitro and to facilitate mucosal healing in mice.

M64HCl has drug-like physicochemical properties. Its molecular weight <500, solubility >100 μM, and log D between 0 and 3 all enhance the probability of good intestinal permeability. Indeed, it is rapidly absorbed after enteral gavage and highly concentrated in the gastric and small intestinal mucosa. M64HCl displays cytotoxicity at 1 mM in IMR-90 human pulmonary fibroblasts and 200 μM in SH-SY5Y human neuronal cells, 10^7-fold higher than the 100 pM that activates FAK. This may explain why we observed no obvious neurotoxicity at therapeutic doses even though M64HCl does cross the blood-brain barrier. The in vivo maximum tolerated single dose of M64HCl is 240 mg/kg. One hour after 240 mg/kg dosing, plasma levels are 176 μg/mL, 3000-fold change in comparison to 58 ng/mL therapeutic plasma concentration after 4 days of 30 mg/kg/day dosing.

Although FAK inhibitors have been used in therapeutic trials to treat

cancer (Infante et al., 2012; Shimizu et al., 2016; Doi et al., 2019; Mak et al., 2019; Mohanty et al., 2020; Dawson et al., 2021), these have not been uniformly successful. The Ames test failed to demonstrate a mutagenic effect of M64HCl, and we did not observe a mitogenic effect in the cell lines studied even at orders of magnitude higher concentrations than effective. Separate studies suggest that FAK activation by this class of small molecules is incomplete and differs in location and downstream signaling consequences from more conventional paradigms of FAK activation by growth factor and matrix proteins (Oncel and Basson, 2022).

M64HCl is a promising drug-like compound. However, its short plasma half-life could require multiple dosing in clinical use. Future studies should focus on designing and optimizing the next generation of lead molecules for a longer half-life, thus potentially developing an effective therapy for NSAID-associated GI mucosal injury that promotes both proximal and distal mucosal healing.

5. Conclusions

M64HCl is a water-soluble drug-like small molecule that activates Focal Adhesion Kinase, promotes gut mucosal healing in mice after injury with minimal toxicity.

Credit author statement

Qinggang Wang: Methodology, Formal analysis, Investigation, Data Curation. Writing – Original Draft, Writing - Review & Editing. **Ricardo Gallardo-Macias**: Methodology, Formal analysis, Data Curation. **Emilie E. Vomhof-DeKrey**: Methodology, Formal analysis, Investigation. **Rashmi Gupta**: Methodology, Formal analysis, Investigation. **Svetlana A Golovko**: Methodology, Formal analysis. **Mikhail Y. Golovko**: Methodology, Formal analysis, Data Curation, Resources. **Sema Oncel**: Investigation, Validation. **Vadim J. Gurvich**: Conceptualization, Resources, Supervision. **Marc D. Basson**: Conceptualization, Resources, Writing - Review & Editing, Supervision.

Declaration of competing interest

The authors declare the following financial interests/personal relationships which may be considered as potential competing interests:The University of North Dakota and the University of Minnesota have filed two patent applications addressing the use of small molecule FAK activators in promoting mucosal healing. Drs. Basson and Gurvich and Gallardo-Macias are named as inventors in at least one of each of these patents. The authors have no other potential competing interests to declare.

Data availability

Data will be made available on request.

Acknowledgments

Histological services were provided by the UND Histology Core Facility supported by NIH/NIGMS awards P20GM113123, U54GM128729, and UND SMHS funds. Supported in part by NIH 3UTGM13-175-02S1 and NIH U01HL152410.

Marc D. Basson and Vadim J Gurvich are co-inventors of two patent applications currently pending that address the use of small molecule FAK activators to promote mucosal healing.

References

Acebrón, I., Righetto, R.D., Schoenherr, C., de Buhr, S., Redondo, P., Culley, J., Rodríguez, C.F., Daday, C., Biyani, N., Llorca, O., Byron, A., Chami, M., Gräter, F., Boskovic, J., Frame, M.C., Stahlberg, H., Lietha, D., 2020. Structural basis of Focal Adhesion Kinase activation on lipid membranes. EMBO J. 39 (19), e104743.

Alam, A., Leoni, G., Wentworth, C.C., Kwal, J.M., Wu, H., Ardita, C.S., Swanson, P.A., Lambeth, J.D., Jones, R.M., Nusrat, A., Neish, A.S., 2014. Redox signaling regulates commensal-mediated mucosal homeostasis and restitution and requires formyl peptide receptor 1. Mucosal Immunol. 7 (3), 645–655.

Ashton, G.H., Morton, J.P., Myant, K., Phesse, T.J., Ridgway, R.A., Marsh, V., Wilkins, J.A., Athineos, D., Muncan, V., Kemp, R., Neufeld, K., Clevers, H., Brunton, V., Winton, D.J., Wang, X., Sears, R.C., Clarke, A.R., Frame, M.C., Sansom, O.J., 2010. Focal adhesion kinase is required for intestinal regeneration and tumorigenesis downstream of Wnt/c-Myc signaling. Dev. Cell 19 (2), 259–269.

Basson, M.D., 2017. Hierarchies of healing in gut mucosal injury. J. Physiol. Pharmacol. 68 (6), 789–795.

Basson, M.D., Sanders, M.A., Gomez, R., Hatfield, J., Vanderheide, R., Thamilselvan, V., Zhang, J., Walsh, M.F., 2006. Focal adhesion kinase protein levels in gut epithelial motility. Am. J. Physiol. Gastrointest. Liver Physiol. 291 (3), G491–G499.

Burridge, K., 2017. Focal adhesions: a personal perspective on a half century of progress. FEBS J. 284 (20), 3355–3361.

Chan, F.K., Kyaw, M., Tanigawa, T., Higuchi, K., Fujimoto, K., Cheong, P.K., Lee, V., Kinoshita, Y., Naito, Y., Watanabe, T., Ching, J.Y., Lam, K., Lo, A., Chan, H., Lui, R., Tang, R.S., Sakata, Y., Tse, Y.K., Takeuchi, T., Handa, O., Nebiki, H., Wu, J.C., Abe, T., Mishiro, T., Ng, S.C., Arakawa, T., 2017a. Similar efficacy of proton-pump inhibitors vs H2-receptor antagonists in reducing risk of upper gastrointestinal bleeding or ulcers in high-risk users of low-dose aspirin. Gastroenterology 152 (1), 105–110 e101.

Chan, F.K.L., Ching, J.Y.L., Tse, Y.K., Lam, K., Wong, G.L.H., Ng, S.C., Lee, V., Au, K.W.L., Cheong, P.K., Suen, B.Y., Chan, H., Kee, K.M., Lo, A., Wong, V.W.S., Wu, J.C.Y., Kyaw, M.H., 2017b. Gastrointestinal safety of celecoxib versus naproxen in patients with cardiothrombotic diseases and arthritis after upper gastrointestinal bleeding (CONCERN): an industry-independent, double-blind, double-dummy, randomised trial. Lancet 389 (10087), 2375–2382.

Chen, W.C., Lin, K.H., Huang, Y.T., Tsai, T.J., Sun, W.C., Chuah, S.K., Wu, D.C., Hsu, P.I., 2017. The risk of lower gastrointestinal bleeding in low-dose aspirin users. Aliment. Pharmacol. Ther. 45 (12), 1542–1550.

Craig, D.H., Owen, C.R., Conway, W.C., Walsh, M.F., Downey, C., Basson, M.D., 2008. Colchicine inhibits pressure-induced tumor cell implantation within surgical wounds and enhances tumor-free survival in mice. J. Clin. Invest. 118 (9), 3170–3180.

Dawson, J.C., Serrels, A., Stupack, D.G., Schlaepfer, D.D., Frame, M.C., 2021. Targeting FAK in anticancer combination therapies. Nat. Rev. Cancer 21 (5), 313–324.

Doi, T., Yang, J.C., Shitara, K., Naito, Y., Cheng, A.L., Sarashina, A., Pronk, L.C., Takeuchi, Y., Lin, C.C., 2019. Phase I study of the focal adhesion kinase inhibitor BI 853520 in Japanese and Taiwanese patients with advanced or metastatic solid tumors. Targeted Oncol. 14 (1), 57–65.

Endo, H., Sakai, E., Kato, T., Umezawa, S., Higurashi, T., Ohkubo, H., Nakajima, A., 2015. Small bowel injury in low-dose aspirin users. J. Gastroenterol. 50 (4), 378–386.

Fujimori, S., Gudis, K., Sakamoto, C., 2010. A review of anti-inflammatory drug-induced gastrointestinal injury: focus on prevention of small intestinal injury. Pharmaceuticals 3 (4), 1187–1201.

Gøtzsche, P.C., 2010. NSAIDs. Clin. Evid. 2010.

Gwee, K.A., Goh, V., Lima, G., Setia, S., 2018. Coprescribing proton-pump inhibitors with nonsteroidal anti-inflammatory drugs: risks versus benefits. J. Pain Res. 11, 361–374.

Higuchi, K., Umegaki, E., Watanabe, T., Yoda, Y., Morita, E., Murano, M., Tokioka, S., Arakawa, T., 2009. Present status and strategy of NSAIDs-induced small bowel injury. J. Gastroenterol. 44 (9), 879–888.

Imhann, F., Bonder, M.J., Vich Vila, A., Fu, J., Mujagic, Z., Vork, L., Tigchelaar, E.F., Jankipersadsing, S.A., Cenit, M.C., Harmsen, H.J., Dijkstra, G., Franke, L., Xavier, R.J., Jonkers, D., Wijmenga, C., Weersma, R.K., Zhernakova, A., 2016. Proton pump inhibitors affect the gut microbiome. Gut 65 (5), 740–748.

Infante, J.R., Camidge, D.R., Mileshkin, L.R., Chen, E.X., Hicks, R.J., Rischin, D., Fingert, H., Pierce, K.J., Xu, H., Roberts, W.G., Shreeve, S.M., Burris, H.A., Siu, L.L., 2012. Safety, pharmacokinetic, and pharmacodynamic phase I dose-escalation trial of PF-00562271, an inhibitor of focal adhesion kinase, in advanced solid tumors. J. Clin. Oncol. 30 (13), 1527–1533.

Iwamoto, J., Mizokami, Y., Saito, Y., Shimokobe, K., Honda, A., Ikegami, T., Matsuzaki, Y., 2014. Small-bowel mucosal injuries in low-dose aspirin users with obscure gastrointestinal bleeding. World J. Gastroenterol. 20 (36), 13133–13138.

Iwamoto, J., Saito, Y., Honda, A., Matsuzaki, Y., 2013. Clinical features of gastroduodenal injury associated with long-term low-dose aspirin therapy. World J. Gastroenterol. 19 (11), 1673–1682.

Kamada, T., Satoh, K., Itoh, T., Ito, M., Iwamoto, J., Okimoto, T., Kanno, T., Sugimoto, M., Chiba, T., Nomura, S., Mieda, M., Hiraishi, H., Yoshino, J., Takagi, A., Watanabe, S., Koike, K., 2021. Evidence-based clinical practice guidelines for peptic ulcer disease 2020. J. Gastroenterol. 56 (4), 303–322.

Kavitt, R.T., Lipowska, A.M., Anyane-Yeboa, A., Gralnek, I.M., 2019. Diagnosis and treatment of peptic ulcer disease. Am. J. Med. 132 (4), 447–456.

Khan, R.I., Yazawa, T., Anisuzzaman, A.S., Semba, S., Ma, Y., Uwada, J., Hayashi, H., Suzuki, Y., Ikeuchi, H., Uchino, M., Maemoto, A., Muramatsu, I., Taniguchi, T., 2014. Activation of focal adhesion kinase via M1 muscarinic acetylcholine receptor is required in restitution of intestinal barrier function after epithelial injury. Biochim. Biophys. Acta 1842 (4), 635–645.

Kyaw, M.H., Otani, K., Ching, J.Y.L., Higashimori, A., Kee, K.M., Watanabe, T., Tse, Y.K., Lee, V., Tanigawa, T., Cheong, P.K., Suen, B.Y., Fujiwara, Y., Lam, K., Arakawa, T., Chan, F.K.L., 2018. Misoprostol heals small bowel ulcers in aspirin users with small bowel bleeding. Gastroenterology 155 (4), 1090–1097 e1091.

Lanas, Á., Carrera-Lasfuentes, P., Arguedas, Y., García, S., Bujanda, L., Calvet, X., Ponce, J., Perez-Aísa, Á., Castro, M., Muñoz, M., Sostres, C., García-Rodríguez, L.A., 2015. Risk of upper and lower gastrointestinal bleeding in patients taking

nonsteroidal anti-inflammatory drugs, antiplatelet agents, or anticoagulants. Clin. Gastroenterol. Hepatol. 13 (5), 906–912 e902.
Lanas, A., García-Rodríguez, L.A., Arroyo, M.T., Gomollón, F., Feu, F., González-Pérez, A., Zapata, E., Bástida, G., Rodrigo, L., Santolaria, S., Güell, M., de Argila, C.M., Quintero, E., Borda, F., Piqué, J.M., 2006. Risk of upper gastrointestinal ulcer bleeding associated with selective cyclo-oxygenase-2 inhibitors, traditional non-aspirin non-steroidal anti-inflammatory drugs, aspirin and combinations. Gut 55 (12), 1731–1738.
Li, J., Lu, Y., Wang, D., Quan, F., Chen, X., Sun, R., Zhao, S., Yang, Z., Tao, W., Ding, D., Gao, X., Cao, Q., Zhao, D., Qi, R., Chen, C., He, L., Hu, K., Chen, Z., Yang, Y., Luo, Y., 2019. Schisandrin B prevents ulcerative colitis and colitis-associated-cancer by activating focal adhesion kinase and influence on gut microbiota in an in vivo and in vitro model. Eur. J. Pharmacol. 854, 9–21.
Lietha, D., Cai, X., Ceccarelli, D.F., Li, Y., Schaller, M.D., Eck, M.J., 2007. Structural basis for the autoinhibition of focal adhesion kinase. Cell 129 (6), 1177–1187.
Lim, D.H., Jung, K., Lee, S.B., Park, I.K., Cha, H.J., Park, J.H., Kim, B.G., Jung, S.W., In Du, J., Kim, J.H., Kim, S.E., Moon, W., In Park, M., Park, S.J., 2020. Non-steroidal anti-inflammatory drug-induced enteropathy as a major risk factor for small bowel bleeding: a retrospective study. BMC Gastroenterol. 20 (1), 178.
Lué, A., Lanas, A., 2016. Protons pump inhibitor treatment and lower gastrointestinal bleeding: balancing risks and benefits. World J. Gastroenterol. 22 (48), 10477–10481.
Maiden, L., 2009. Capsule endoscopic diagnosis of nonsteroidal antiinflammatory drug-induced enteropathy. J. Gastroenterol. 44 (Suppl. 19), 64–71.
Maiden, L., Thjodleifsson, B., Seigal, A., Bjarnason II, Scott, D., Birgisson, S., Bjarnason, I., 2007. Long-term effects of nonsteroidal anti-inflammatory drugs and cyclooxygenase-2 selective agents on the small bowel: a cross-sectional capsule enteroscopy study. Clin. Gastroenterol. Hepatol. 5 (9), 1040–1045.
Mak, G., Soria, J.C., Blagden, S.P., Plummer, R., Fleming, R.A., Nebot, N., Zhang, J., Mazumdar, J., Rogan, D., Gazzah, A., Rizzuto, I., Greystoke, A., Yan, L., Tolson, J., Auger, K.R., Arkenau, H.T., 2019. A phase Ib dose-finding, pharmacokinetic study of the focal adhesion kinase inhibitor GSK2256098 and trametinib in patients with advanced solid tumours. Br. J. Cancer 120 (10), 975–981.
Marlicz, W., Loniewski, I., Grimes, D.S., Quigley, E.M., 2014. Nonsteroidal anti-inflammatory drugs, proton pump inhibitors, and gastrointestinal injury: contrasting interactions in the stomach and small intestine. Mayo Clin. Proc. 89 (12), 1699–1709.
Meltzer, A.C., Ward, M.J., Gralnek, I.M., Pines, J.M., 2014. The cost-effectiveness analysis of video capsule endoscopy compared to other strategies to manage acute upper gastrointestinal hemorrhage in the ED. Am. J. Emerg. Med. 32 (8), 823–832.
Miyake, K., Akimoto, T., Hanada, Y., Nagoya, H., Kodaka, Y., Ueki, N., Kusunoki, M., Kawagoe, T., Futagami, S., Takahashi, Y., Takano, H., Sakamoto, C., 2015. Proton pump inhibitors are associated with lower gastrointestinal tract bleeding in low-dose aspirin users with ischaemic heart disease. Dig. Liver Dis. 47 (9), 757–762.
Mohanty, A., Pharaon, R.R., Nam, A., Salgia, S., Kulkarni, P., Massarelli, E., 2020. FAK-targeted and combination therapies for the treatment of cancer: an overview of phase I and II clinical trials. Expet Opin. Invest. Drugs 29 (4), 399–409.
Oncel, S., Basson, M.D., 2. ZINC40099027 promotes monolayer circular defect closure by a novel pathway involving cytosolic activation of focal adhesion kinase and downstream paxillin and ERK1/2. Cell Tissue Res. 390, 261–279.
Oncel, S., Gupta, R., Wang, Q., Basson, M.D., 2021. ZINC40099027 promotes gastric mucosal repair in ongoing aspirin-associated gastric injury by activating focal adhesion kinase. Cells 10 (4).
Owen, K.A., Abshire, M.Y., Tilghman, R.W., Casanova, J.E., Bouton, A.H., 2011. FAK regulates intestinal epithelial cell survival and proliferation during mucosal wound healing. PLoS One 6 (8), e23123.
Park, S.C., Chun, H.J., Kang, C.D., Sul, D., 2011. Prevention and management of non-steroidal anti-inflammatory drugs-induced small intestinal injury. World J. Gastroenterol. 17 (42), 4647–4653.
Raschka, S., More, S.K., Devadoss, D., Zeng, B., Kuhn, L.A., Basson, M.D., 2018. Identification of potential small-molecule protein-protein inhibitors of cancer metastasis by 3D epitope-based computational screening. J. Physiol. Pharmacol. 69 (2).
Rashmi, S.K.More, Wang, Q., Vomhof-DeKrey, E.E., Porter, J.E., Basson, M.D., 2021. ZINC40099027 activates human focal adhesion kinase by accelerating the enzymatic activity of the FAK kinase domain. Pharmacol Res Perspect 9 (2), e00737.
Rostom, A., Dube, C., Wells, G., Tugwell, P., Welch, V., Jolicoeur, E., McGowan, J., 2002. Prevention of NSAID-induced gastroduodenal ulcers. Cochrane Database Syst. Rev. 4, Cd002296.
Rostom, A., Muir, K., Dubé, C., Jolicoeur, E., Boucher, M., Joyce, J., Tugwell, P., Wells, G.W., 2007. Gastrointestinal safety of cyclooxygenase-2 inhibitors: a Cochrane Collaboration systematic review. Clin. Gastroenterol. Hepatol. 5 (7), 818–828, 828.e811-815; quiz 768.
Satoh, H., Amagase, K., Takeuchi, K., 2012. Exacerbation of nonsteroidal anti-inflammatory drug-induced small intestinal lesions by antisecretory drugs in rats: the role of intestinal motility. J. Pharmacol. Exp. Therapeut. 343 (2), 270–277.
Scarpignato, C., Bjarnason, I., 2019. Drug-induced small bowel injury: a challenging and often forgotten clinical condition. Curr. Gastroenterol. Rep. 21 (11), 55.
Shimizu, T., Fukuoka, K., Takeda, M., Iwasa, T., Yoshida, T., Horobin, J., Keegan, M., Vaickus, L., Chavan, A., Padval, M., Nakagawa, K., 2016. A first-in-Asian phase 1 study to evaluate safety, pharmacokinetics and clinical activity of VS-6063, a focal adhesion kinase (FAK) inhibitor in Japanese patients with advanced solid tumors. Cancer Chemother. Pharmacol. 77 (5), 997–1003.
Shiratsuchi, H., Basson, M.D., 2004. Extracellular pressure stimulates macrophage phagocytosis by inhibiting a pathway involving FAK and ERK. Am. J. Physiol. Cell Physiol. 286 (6), C1358–C1366.
Sugano, K., Choi, M.G., Lin, J.T., Goto, S., Okada, Y., Kinoshita, Y., Miwa, H., Chiang, C.E., Chiba, T., Hori, M., Fukushima, Y., Kim, H.S., Chang, C.Y., Date, M., 2014. Multinational, double-blind, randomised, placebo-controlled, prospective study of esomeprazole in the prevention of recurrent peptic ulcer in low-dose acetylsalicylic acid users: the LAVENDER study. Gut 63 (7), 1061–1068.
Sugimori, S., Watanabe, T., Tabuchi, M., Kameda, N., Machida, H., Okazaki, H., Tanigawa, T., Yamagami, H., Shiba, M., Watanabe, K., Tominaga, K., Fujiwara, Y., Oshitani, N., Koike, T., Higuchi, K., Arakawa, T., 2008. Evaluation of small bowel injury in patients with rheumatoid arthritis by capsule endoscopy: effects of anti-rheumatoid arthritis drugs. Digestion 78 (4), 208–213.
Syer, S.D., Blackler, R.W., Martin, R., de Palma, G., Rossi, L., Verdu, E., Bercik, P., Surette, M.G., Aucouturier, A., Langella, P., Wallace, J.L., 2015. NSAID enteropathy and bacteria: a complicated relationship. J. Gastroenterol. 50 (4), 387–393.
Szabó, I.L., Mátics, R., Hegyi, P., Garami, A., Illés, A., Sarlós, P., Bajor, J., Szűcs, A., Mosztbacher, D., Márta, K., Szemes, K., Csekő, K., Kővári, B., Rumbus, Z., Vincze, Á., 2017. PPIs prevent aspirin-induced gastrointestinal bleeding better than H2RAs. A systematic review and meta-analysis. J. Gastrointestin. Liver. Dis. 26 (4), 395–402.
Taha, A.S., McCloskey, C., McSkimming, P., McConnachie, A., 2018. Misoprostol for small bowel ulcers in patients with obscure bleeding taking aspirin and non-steroidal anti-inflammatory drugs (MASTERS): a randomised, double-blind, placebo-controlled, phase 3 trial. Lancet Gastroenterol. Hepatol. 3 (7), 469–476.
Tai, F.W.D., McAlindon, M.E., 2018. NSAIDs and the small bowel. Curr. Opin. Gastroenterol. 34 (3), 175–182.
Teutsch, B., Boros, E., Váncsa, S., Váradi, A., Frim, L., Kiss, S., Dembrovszky, F., Helyes, Z., Patrícia, S., Péter, H., Erőss, B., 2021. Mucoprotective drugs can prevent and treat nonsteroidal anti-inflammatory drug-induced small bowel enteropathy: a systematic review and meta-analysis of randomized controlled trials. Therap. Adv. Gastroenterol. 14, 17562848211038772.
Thamilselvan, V., Craig, D.H., Basson, M.D., 2007. FAK association with multiple signal proteins mediates pressure-induced colon cancer cell adhesion via a Src-dependent PI3K/Akt pathway. Faseb. J. 21 (8), 1730–1741.
Tran-Duy, A., Vanmolkot, F.H., Joore, M.A., Hoes, A.W., Stehouwer, C.D., 2015. Should patients prescribed long-term low-dose aspirin receive proton pump inhibitors? A systematic review and meta-analysis. Int. J. Clin. Pract. 69 (10), 1088–1111.
Usechak, P., Gates, A., Webster, C.R., 2008. Activation of focal adhesion kinase and JNK contributes to the extracellular matrix and cAMP-GEF mediated survival from bile acid induced apoptosis in rat hepatocytes. J. Hepatol. 49 (2), 251–261.
Wallace, J.L., 2001. Pathogenesis of NSAID-induced gastroduodenal mucosal injury. Best Pract. Res. Clin. Gastroenterol. 15 (5), 691–703.
Wallace, J.L., 2008. Prostaglandins, NSAIDs, and gastric mucosal protection: why doesn't the stomach digest itself? Physiol. Rev. 88 (4), 1547–1565.
Wallace, J.L., 2012. NSAID gastropathy and enteropathy: distinct pathogenesis likely necessitates distinct prevention strategies. Br. J. Pharmacol. 165 (1), 67–74.
Wallace, J.L., Syer, S., Denou, E., de Palma, G., Vong, L., McKnight, W., Jury, J., Bolla, M., Bercik, P., Collins, S.M., Verdu, E., Ongini, E., 2011. Proton pump inhibitors exacerbate NSAID-induced small intestinal injury by inducing dysbiosis. Gastroenterology 141 (4), 1314–1322, 1322.e1311-1315.
Walsh, M.F., Ampasala, D.R., Hatfield, J., Vander Heide, R., Suer, S., Rishi, A.K., Basson, M.D., 2008. Transforming growth factor-beta stimulates intestinal epithelial focal adhesion kinase synthesis via Smad- and p38-dependent mechanisms. Am. J. Pathol. 173 (2), 385–399.
Wang, J., Wen, T., Li, Z., Che, X., Gong, L., Yang, X., Zhang, J., Tang, H., He, L., Qu, X., Liu, Y., 2019a. MicroRNA-1224 inhibits tumor metastasis in intestinal-type gastric cancer by directly targeting FAK. Front. Oncol. 9, 222.
Wang, Q., Gallardo-Macias, R., Rashmi, Golovko, M.Y., Elsayed, A.A.R., More, S.K., Oncel, S., Gurvich, V.J., Basson, M.D., 2021. Discovery of novel small-molecule FAK activators promoting mucosal healing. ACS Med. Chem. Lett. 12 (3), 356–364.
Wang, Q., More, S.K., Vomhof-DeKrey, E.E., Golovko, M.Y., Basson, M.D., 2019b. Small molecule FAK activator promotes human intestinal epithelial monolayer wound closure and mouse ulcer healing. Sci. Rep. 9 (1), 14669.
Wang, S., Basson, M.D., 2011. Akt directly regulates focal adhesion kinase through association and serine phosphorylation: implication for pressure-induced colon cancer metastasis. Am. J. Physiol. Cell Physiol. 300 (3), C657–C670.
Washio, E., Esaki, M., Maehata, Y., Miyazaki, M., Kobayashi, H., Ishikawa, H., Kitazono, T., Matsumoto, T., 2016. Proton pump inhibitors increase incidence of nonsteroidal anti-inflammatory drug-induced small bowel injury: a randomized, placebo-controlled trial. Clin. Gastroenterol. Hepatol. 14 (6), 809–815 e801.
Watanabe, T., Fujiwara, Y., Chan, F.K.L., 2020. Current knowledge on non-steroidal anti-inflammatory drug-induced small-bowel damage: a comprehensive review. J. Gastroenterol. 55 (5), 481–495.
Watanabe, T., Sugimori, S., Kameda, N., Machida, H., Okazaki, H., Tanigawa, T., Watanabe, K., Tominaga, K., Fujiwara, Y., Oshitani, N., Higuchi, K., Arakawa, T., 2008. Small bowel injury by low-dose enteric-coated aspirin and treatment with misoprostol: a pilot study. Clin. Gastroenterol. Hepatol. 6 (11), 1279–1282.
Xie, Y., Han, K.H., Grainger, N., Li, W., Corrigan, R.D., Perrino, B.A., 2018. A role for focal adhesion kinase in facilitating the contractile responses of murine gastric fundus smooth muscles. J. Physiol. 596 (11), 2131–2146.
Yamagata, M., Hiraishi, H., 2007. [Prevalence and incidence of NSAID-induced gastrointestinal ulcers and bleeding]. Nihon Rinsho 65 (10), 1749–1753.
Zeng, B., Devadoss, D., Wang, S., Vomhof-DeKrey, E.E., Kuhn, L.A., Basson, M.D., 2017. Inhibition of pressure-activated cancer cell adhesion by FAK-derived peptides. Oncotarget 8 (58), 98051–98067.
Zhang, S., Chao, G.Q., Lu, B., 2013. Proton pump inhibitors are not the key for therapying non-steroidal anti-inflammatory drugs-induced small intestinal injury. Rheumatol. Int. 33 (10), 2513–2521.